

Holm Altenbach
Andreas Öchsner
Editors



International Centre
for Mechanical Sciences

Cellular and Porous Materials in Structures and Processes

CISM Courses and Lectures, vol. 521



SpringerWienNewYork

 SpringerWienNewYork

CISM COURSES AND LECTURES

Series Editors:

The Rectors

Giulio Maier - Milan

Franz G. Rammerstorfer - Wien

Jean Salençon - Palaiseau

The Secretary General

Bernhard Schrefler - Padua

Executive Editor

Paolo Serafini - Udine

The series presents lecture notes, monographs, edited works and proceedings in the field of Mechanics, Engineering, Computer Science and Applied Mathematics.

Purpose of the series is to make known in the international scientific and technical community results obtained in some of the activities organized by CISM, the International Centre for Mechanical Sciences.

INTERNATIONAL CENTRE FOR MECHANICAL SCIENCES

COURSES AND LECTURES - No. 521



CELLULAR AND POROUS MATERIALS IN STRUCTURES AND PROCESSES

EDITED BY

HOLM ALTENBACH

MARTIN-LUTHER-UNIVERSITÄT, HALLE-WITTENBERG, GERMANY

ANDREAS ÖCHSNER

TECHNICAL UNIVERSITY OF MALAYSIA, MALAYSIA

SpringerWienNewYork

This volume contains 141 illustrations

This work is subject to copyright.
All rights are reserved,
whether the whole or part of the material is concerned
specifically those of translation, reprinting, re-use of illustrations,
broadcasting, reproduction by photocopying machine
or similar means, and storage in data banks.

© 2010 by CISM, Udine

Printed in Italy

SPIN 80016755

All contributions have been typeset by the authors.

ISBN 978-3-7091-0296-1 SpringerWienNewYork

PREFACE

Metallic and polymer foams are widely used in modern industries, e.g., the aircraft and the automotive industries, but also with other application fields like biomechanics. The reason for this is some specific properties of these advanced materials. They are very light, but the specific strength is comparable with the classical structural materials. If they are applied as sandwiches, the specific properties can be even much better. In addition, they are able to absorb energy which allows the use of these materials as crash elements.

In general, technological parameters in foam production are adjusted such that a uniform effective foam density is achieved throughout the products. Some technologies, e.g., injecting foam in a cavity or filling a mold with foam by an expansion process, naturally result in non-uniform distributions of the effective density. These inhomogeneities of the effective foam density may be exploited in structural design, essentially treating the foam as a functionally graded material.

FGMs are composite materials where the composition or the microstructure is locally varied so that a certain variation of the local material properties is achieved. Modern FGMs are constructed for complex requirements, such as the heat shield of a rocket or implants for humans. In these cases the analysis of the material and the structures made of FGMs cannot be only limited to the mechanical behavior. FGMs can be modeled as a porous material with non-homogeneous distribution of porosity.

Engineering structures made of porous materials, especially metal foams, have been used in different applications in the last decades. A metal foam is a cellular structure consisting of a solid metal, for example aluminium, steel, copper, etc., containing a large volume fraction of gas-filled pores. There are two types of metal foams. One is the closed-cell foam, while the second one is the open-cell foam. The defining characteristics of metal foams are a very high porosity: typically well over 80%, 90% and even 98% of the volume consists of void spaces.

The course "Cellular and Porous Materials: Modeling - Testing - Application" was devoted to cellular and porous materials, and the modeling and simulation of the material behavior, but also the structural analysis of structures made of foams, the testing and the appli-

cations. The main question was on which scale one has to model the material. It is well-known that there are as a minimum three scales:

- *micro-mechanical scale*

The starting point in this case is a unit cell which can be open or closed (open-cell foams, closed-cell foams). The description is very fine (the unit cell is modeled by beams, plates or shells), but the computational effort increases significantly if high accuracy (e.g. in the case of plasticity) is required, and the identification of the properties is still under question.

- *meso-mechanical scale*

Now the starting point is an agglomerate of cells (representative volume), computational effort is quite expensive. In addition, the periodicity assumption is under question.

- *macro-mechanical scale*

Now one has the size of structural elements or specimens. Using standard numerical techniques the computational effort is as in the case of classical structural materials. The disadvantage is that "smeared" properties should be introduced (that means the constitutive behavior will be represented by phenomenological equations) and local effects cannot be investigated.

During the 6 lectures

- *Fracture Mechanics of Foams (Livi Marsavina)*
- *Finite Element Modeling of Foams (Thomas Darner)*
- *Plasticity of Three-dimensional Foams (Andreas Öchsner)*
- *Thin-walled Structures Made of Foams (Holm Altenbach)*
- *Plasticity of Porous and Powder Metals (Sergei Alexandrov)*
- *Impact of Cellular Materials (Henry Tan)*

the advantages and disadvantages of each approach were discussed.

The basics of the analysis of structures made of foams is the continuum mechanics. Briefly were presented the foundations. In addition, the introduction in the theory of elasticity and plasticity was given. Special attention was paid to the yield criteria, to anisotropy and to the different behavior in tension and compression. Many structural elements made of foams can be presented by beam, plate or shell models. As an example, a plate theory based on the direct approach was presented. One of the basic elements of this theory is the effective property concept. Such a theory is suitable for the global analysis of plates (deflections, frequencies, etc.).

Holm Altenbach and Andreas Öchsner

CONTENTS

Fracture Mechanics of Foams <i>by L. Marsavina</i>	1
1 Fundamentals of Fracture Mechanics	1
1.1 Introduction	1
1.2 Linear Elastic Fracture Mechanics	3
1.3 Crack tip stress and displacement fields in anisotropic materials	12
2 Experimental Determination of Fracture Toughness of Foam Materials	16
2.1 Tear Test for Flexible Cellular Materials	17
2.2 Standard Test Methods for Plane-Strain Fracture Toughness and Strain Energy Release Rate of Plastic Materials	18
2.3 Fracture Toughness Experimental Results	24
2.4 Impact Fracture Toughness	29
3 Micromechanical Models for Foams Fracture	34
4 Concluding Remarks	42
Bibliography	43
Finite Element Modeling of Foams <i>by Th. Daxner</i>	47
1 Introduction	47
2 Homogenization and the Unit Cell Method	49
3 Micro-Mechanical Finite Element Models of Cellular Materials	57
3.1 Introduction	57

3.2	Open-Cell Foams	63
3.3	Closed-Cell Foams	67
3.4	Open-Cell Foams with Hollow Struts.	72
4	Micro-Mechanical Models — Methods and Results	73
4.1	Elastic Properties	74
4.2	Yielding	75
4.3	Buckling	80
4.4	Densification	91
4.5	Fracture	93
5	Optimization of Foam Density Distribution	96
6	Summary	98
	Bibliography	98

Plasticity of Three-dimensional Foams

by A. Öchsner **107**

1	Fundamentals of Continuum Mechanics	107
1.1	Stress Tensor and Decomposition	107
1.2	Invariants	109
1.3	Constitutive Equations	112
1.4	Linear Elastic Behaviour: Generalised Hooke's Law for Isotropic Materials	113
2	Constitutive Relationships for Pressure Sensitive Materials: Systematic Overview	119
3	Simple Cubic Cell Models based on Beams and Shells for Open and Closed Cell Materials	129
3.1	Relative Density	133
3.2	Geometrical Moment of Inertia	135
3.3	Young's Modulus	135
3.4	Shear Modulus and Poisson's Ratio	136

3.5	Yield Stress	140
4	Procedures to Determine the Influence of the Hydrostatic Stress on the Yield Behaviour	141
5	Implementation of New Constitutive Equations into Commercial Finite Element Codes	146
5.1	One-Dimensional Drucker-Prager Yield Condition	146
5.2	Integration of the Constitutive Equations	148
5.3	Mathematical Derivation of the Fully Implicit Backward Euler Algorithm	152
5.4	Example Problem: Return Mapping for Ideal Plasticity and Linear Hardening	158
	Bibliography	164

Thin-walled Structures Made of Foams
by H. Altenbach and V.A. Eremeyev **167**

1	Introduction	168
1.1	Plates as Structural Elements	168
1.2	Foams as a Material for Structural Elements . . .	169
2	Direct Two-dimensional Plate Theory	171
2.1	Classical Approaches in the Plate Theory	171
2.2	Governing Equations	173
2.3	Material-independent Equations	174
2.4	Two-dimensional Constitutive Equations	175
2.5	Basic Equations in Cartesian Coordinates	176
3	Stiffness Identification	179
3.1	Orthotropic Material Behavior	180
3.2	Classical Stiffness Values	181
3.3	Non-classical Stiffness Values	183
3.4	Special Case – Isotropic Behavior	185

4	Examples of Effective Stiffness Properties Estimates	186
4.1	Homogeneous Plate	186
4.2	Classical Sandwich Plate in Reissner's Sense . . .	187
4.3	Functionally Graded Materials and Foams	188
4.4	On the Plates Made of Nanofoams	193
5	Symmetric Orthotropic Plate - Static Case	196
5.1	Bending Problem - One-dimensional Case	198
5.2	Bending Problem - Two-dimensional Case	198
5.3	Bending of an Isotropic Plate	199
5.4	Bending of an Elastic Plate Made of FGM (Symmetric Case)	200
6	Dynamics of Plates Made of an Elastic Foam	201
6.1	Equations of Motion for a Symmetric Isotropic Plate	201
6.2	Free Oscillations and Dispersion curves of a Rectangular Plate	203
7	Plate Made of a Linear Viscoelastic Material	209
7.1	Constitutive Equations	209
7.2	Effective Properties	210
7.3	Bounds for the Eigen-values	214
7.4	Quasi-static Behavior of a Symmetric Orthotropic Plate	215
7.5	Examples of Effective Stiffness Relaxation Functions	217
7.6	Bending of a Viscoelastic Plate	222
8	Plate Theory Deduced from the Cosserat Continuum	226
8.1	Two-dimensional Governing Equations	226
8.2	Reduction of the Three-dimensional Micropolar Equations	228
9	Summary	232
	Bibliography	234

Plasticity of Porous and Powder Metals	
<i>by S. Alexandrov</i>	243
1 Introduction	243
2 Fundamentals of the Theory of Plasticity	245
2.1 Rigid Perfectly/Plastic Solids	245
2.2 Rigid Plastic Hardening Solids	252
2.3 Rigid Viscoplastic Solids	253
2.4 Maximum Friction Law and Singular Velocity Fields (Rigid Perfectly/Plastic Material)	254
2.5 Maximum Friction Law and Other Models of Pressure-independent Plasticity	261
3 Plasticity Theory for Porous and Powder Metals Based on the Associated Flow Rule	262
3.1 Preliminaries	262
3.2 Yield Criteria and the Associated Flow Rule for Porous and Powder Materials	265
3.3 Additional Remarks on the Yield Criteria	270
3.4 Simple Analytic Example	271
4 Plasticity Theory for Porous and Powder Metals Based on Non-associated Flow Rules	277
4.1 Stress Equations	277
4.2 Kinematic Theories	280
4.3 The Coaxial Model	281
4.4 The Double-shearing Model	282
4.5 The Double-slip and Rotation Model	284
5 Qualitative Behavior of Plastic Solutions for Porous and Powder Metals in the Vicinity of Frictional Interfaces	285
5.1 Preliminaries	285
5.2 Statement of the Problem	285

5.3	Solution for Stresses	289
5.4	Solutions for Velocities	290
5.5	Frictional Boundary Condition	292
5.6	Solution for Pressure-independent Plasticity . . .	299
5.7	Singularity in Velocity Fields	300
6	Applications	302
	Bibliography	305
	Impact of Cellular Materials	
	<i>by H. Tan and S. Qu</i>	309
1	Introduction	309
2	Wave Propagation in a Cellular Rod	311
3	Rigid Object Strikes on a Cellular Rod of Fixed End	316
	3.1 Basic Assumptions	316
	3.2 Shock Wave Analysis	317
4	Rigid Object Strikes on a Free Cellular Rod	325
5	Concluding Remarks	333
	Bibliography	333

Fracture Mechanics of Cellular Solids

Liviu Marsavina*

* POLITEHNICA University of Timisoara, Romania

Abstract Most of foam materials crush in compression, while in tension fail by propagating of single cracks. Rigid polymer foams have a linear-elastic behavior in tension up to the brittle fracture, so they can be treated using Linear Elastic Fracture Mechanics. This chapter presents the Linear Elastic Fracture Mechanics parameters and criteria with application for foam materials. Methods for experimental determination for tear strength and fracture toughness are presented. The obtained experimental results are discussed and compared with other published data. Main micromechanical models for predicting fracture toughness of cellular materials are also discussed.

1 Fundamentals of Fracture Mechanics

1.1 Introduction

Most of the structures contain small flaws whose size and distribution are dependent on the material and its processing. These flaws can extend rapidly at applied load levels which are nominally well within the linear elastic part of load-displacement response of the structure. Several structural failures can be associated with the fracture of one or more of its components. When such events occur, they are mostly unexpected, sudden, and unfortunate, and it is natural for us to focus attention on minimizing the undesired consequences when designing and analyzing modern-day structures. The study of crack behavior, prevention and analysis of fracture of materials is known as fracture mechanics. The goal of fracture mechanics is to predict the critical loads that will cause catastrophic failure in a structure or component. The influence of pre-existing cracks on the strength of components needs to be understood and quantified. The initiation and growth of crack like defects during service (fatigue, creep) needs to be understood and quantified. A defect tolerant design and maintenance philosophy is necessary to be developed.

The most famous failure produced by foam fracture is the Space Shuttle Columbia disaster occurred on February 1, 2003, when disintegrated over

Palestine, Texas during re-entry into the Earth's atmosphere, with the loss of all seven crew members. The Columbia accident was a result of damage sustained during launch when a piece of foam insulation with the size of a small briefcase broke off the Space Shuttle external tank under the aerodynamic forces of launch. The debris struck the leading edge of the left wing, damaging the Shuttle's thermal protection system (TPS), Fig. 1, which protects it from heat generated with the atmosphere during re-entry. While Columbia was still in orbit, some engineers suspected damage, but

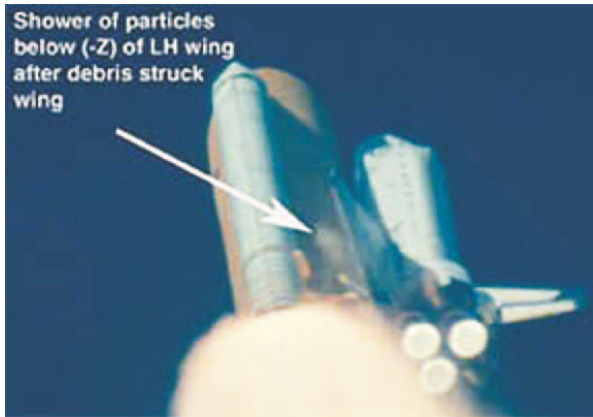


Figure 1. The foam from the fuel tank hit the left wing of the shuttle KSC-03PD-0250: <http://mediaarchive.ksc.nasa.gov/>

NASA managers limited the investigation, on the grounds that little could be done even if problems were found. NASA engineers reviewed the launch tapes to reveal a 500 mm piece of hardened insulation foam breaking off the main fuel tank and hitting the shuttle's left wing. When the shuttle broke up during reentry, no one could ascertain if it was because of the damaged wing hit by the foam.

The reason to apply fracture mechanics for cellular materials can be summarized as follows:

- The Columbia disaster is an example of catastrophic failure caused by fracture of foam,
- The rigid foams have a brittle fracture in tension, and the failure is produced by single crack propagation,
- LEFM approaches describe the fracture of rigid polyurethane foams and expanded polystyrene foams, while tearing occurs for semi-rigid low-densities polyethylene, or flexible polyurethane foams.

1.2 Linear Elastic Fracture Mechanics

Many textbooks present the principle of linear elastic fracture mechanics (LEFM) (Broek, 1986; Ewalds and Wanhill, 1989; Anderson, 1995; Shukla, 2005). Here only a review of the main fracture criteria for LEFM will be presented.

Griffith Energy. Griffith (1921) proposed an energy balance approach to study the fracture phenomenon in cracked bodies. He proposed that the reduction in strain energy of a body when the crack propagates could be equated to the increase in surface energy due to the increase in the surface area. The Griffith theory assumed that the fracture strength was limited by the existence of initial cracks and that brittle materials contain elliptical microcracks, which introduce high stress concentrations near their tips. He developed a relationship between crack length (a), surface energy connected with traction-free crack surfaces ($2\gamma_e$), Young's modulus E and applied stress σ , which is given by

$$\sigma\sqrt{a} = \sqrt{\frac{2E\gamma_e}{\pi}} \quad (1)$$

According with Eq. (1), which is valid for plane stress, the fracture occurs when the product $\sigma\sqrt{a}$ reaches a particular value depending on material constants E and γ_e .

Later Irwin (1957) introduced the energy release rate \mathcal{G} defined as the rate of change in potential energy with crack area for a linear elastic material. For an infinite plate (Fig. 2), with a crack of length $2a$, loaded with a remote tensile stress σ the energy release rate is:

$$\mathcal{G} = \frac{\pi\sigma^2 a}{E} \quad \text{- for plane stress} \quad (2)$$

$$\mathcal{G} = \frac{\pi\sigma^2 a}{E}(1 - \nu^2) \quad \text{- for plane strain} \quad (3)$$

Irwin (1957) proposed a fracture criteria based on the energy release rate which states that the fracture occurs when the energy release rate reaches a critical value \mathcal{G}_c , known also as fracture toughness

$$\mathcal{G} = \mathcal{G}_c \quad (4)$$

The critical combination of stress and crack length for fracture occurrence can be expressed in the form

$$\mathcal{G}_c = \frac{\pi\sigma_f^2 a_c}{E} \quad (5)$$

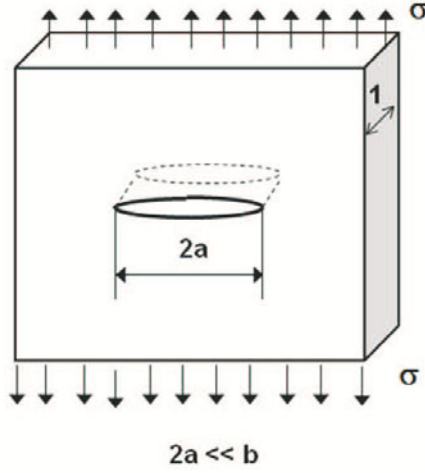


Figure 2. Crack of length $2a$ in an infinite plate remote loaded with tensile stress σ

where σ_f represents the fracture stress and a_c is the critical crack length. Eq. (1) can also be expressed in the form

$$\frac{\pi\sigma^2 a}{E} = 2\gamma_e \quad \text{- for plane stress} \quad (6)$$

$$\frac{\pi\sigma^2 a}{E}(1 - \nu^2) = 2\gamma_e \quad \text{- for plane strain} \quad (7)$$

where the left hand side represents the energy release rate \mathcal{G} , while the right hand side represents the energy needed for incremental crack growth. In addition, it is a measure of resistance to crack advance. So, the condition for unstable crack growth occurs when the energy available for crack extension (crack driving force) equals the resistance of the material to crack advance

$$\mathcal{G} = \mathcal{R} \quad (8)$$

and is graphically represented in Fig. 3.

Orowan (1955) extended the Griffith criterion valid for brittle materials to materials with limited plastic deformations at the crack tip. He postulated that the resistance to crack growth in engineering materials is equal to the sum of elastic surface energy γ_e and the plastic dissipation or plastic

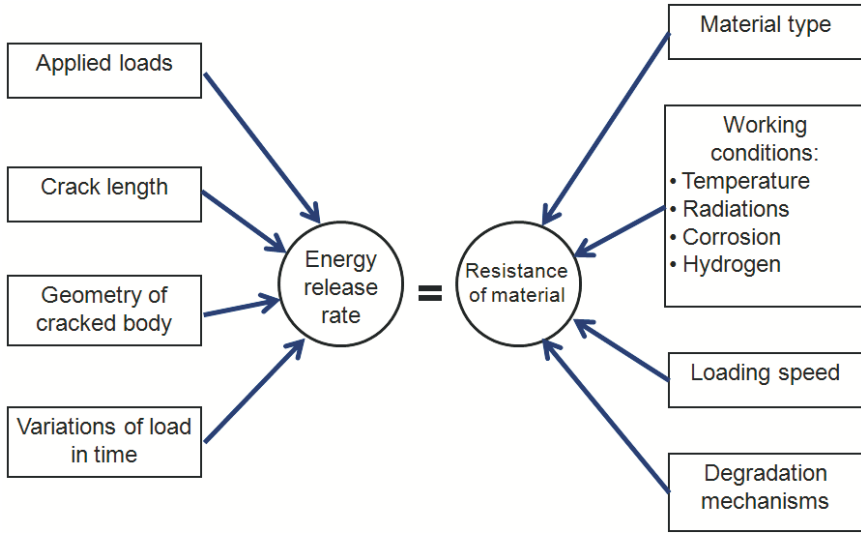


Figure 3. Unstable crack growth condition

work γ_p accompanying crack extension

$$\frac{\pi\sigma^2 a}{E} = 2(\gamma_e + \gamma_p) \quad (9)$$

Asymptotic stress field at the crack tip. In general, consideration of three different loading symmetries is sufficient to decompose any arbitrary loading with respect to a crack, Fig. 4. Mode I corresponds to opening mode, Mode II to in-plane shear and Mode III to out - of - plane shear. In most engineering applications the brittle fracture of structures occurs in Mode I.

According with linear elastic fracture mechanics approach the stress field near the crack tip depends on the crack length a , applied stress σ and a coefficient β which accounts for the geometry of cracked body (finite size, geometric features) and type of loading (tensile, bending, torsion). These are expressed by the Stress Intensity Factor (SIF)

$$K_I = \beta\sigma\sqrt{\pi a} \quad (10)$$

and represents the strength of the stress singularity near the crack tip. The nature of the stress field near the crack tip in a linearly elastic solid

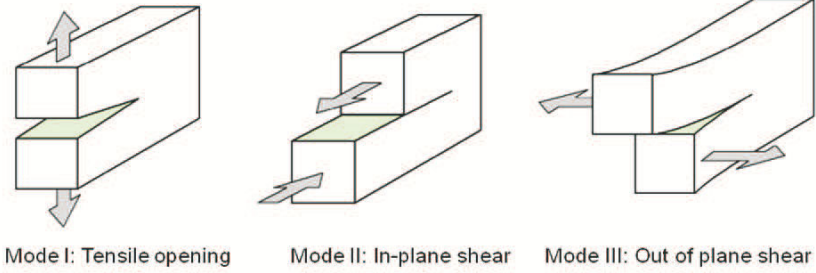


Figure 4. Types of loadings

was established through the efforts of Westergaard (1939); Irwin (1957); Williams (1957) and many other investigators.

For a homogeneous, isotropic, and linearly elastic solid, the structure of the solutions to the equations of equilibrium subjected to traction-free crack surfaces can easily be determined for each of the three modes of loading. This stress field in the vicinity of the crack, cf. Fig. 5 for general mixed mode loading can be written in the following form

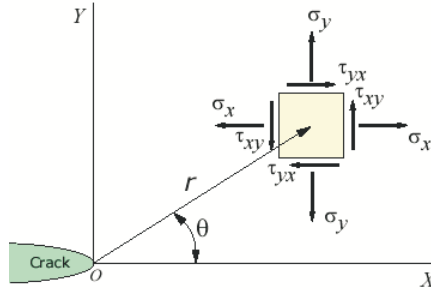


Figure 5. Stress components near crack tip

$$\sigma_{ij}(r, \theta) = \frac{1}{\sqrt{2\pi r}} [K_I f_{ij}^I(\theta) + K_{II} f_{ij}^{II}(\theta) + K_{III} f_{ij}^{III}(\theta)] + \text{higher order terms}, \quad (11)$$

where r, θ are the polar coordinates defining the position of an element in front of a crack tip, cf. Fig. 5, K_I, K_{II} and K_{III} are the Stress Intensity Factors corresponding to the three modes of loading, and $f_{ij}^I, f_{ij}^{II}, f_{ij}^{III}$ are non-dimensional functions indicated in Table 1. The stress field described by Eq. (11) shows that at the crack tip the stresses are theoretically infinite.

Table 1. Non-dimensional functions

f_{ij}	Mode I	Mode II	Mode III
f_{xx}	$\cos \frac{\theta}{2} \left(1 - \sin \frac{\theta}{2} \sin \frac{3\theta}{2} \right)$	$-\sin \frac{\theta}{2} \left(2 + \cos \frac{\theta}{2} \cos \frac{3\theta}{2} \right)$	0
f_{yy}	$\cos \frac{\theta}{2} \left(1 + \sin \frac{\theta}{2} \sin \frac{3\theta}{2} \right)$	$\sin \frac{\theta}{2} \cos \frac{\theta}{2} \cos \frac{3\theta}{2}$	0
f_{zz}	$\begin{cases} 0 & - \text{pl. stress} \\ \nu(\sigma_{xx} + \sigma_{yy}) & - \text{pl. strain} \end{cases}$	$\begin{cases} 0 & - \text{pl. stress} \\ \nu(\sigma_{xx} + \sigma_{yy}) & - \text{pl. strain} \end{cases}$	0
f_{xy}	$\sin \frac{\theta}{2} \cos \frac{\theta}{2} \cos \frac{3\theta}{2}$	$\cos \frac{\theta}{2} \left(1 - \sin \frac{\theta}{2} \sin \frac{3\theta}{2} \right)$	0
f_{xz}	0	0	$-\sin \frac{\theta}{2}$
f_{yz}	0	0	$\cos \frac{\theta}{2}$

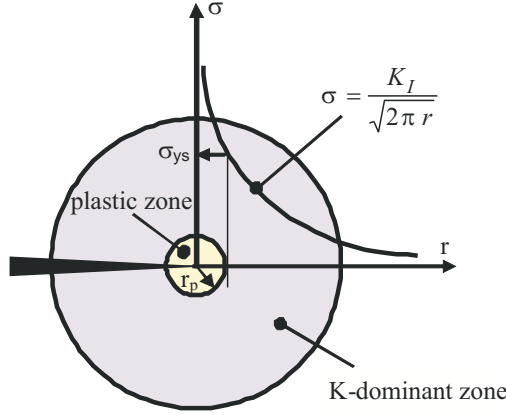


Figure 6. Validity of linear elastic stress field

Most engineering materials when the actual stress reaches the yield stress (σ_{ys}) and have a finite strength. The damaged zone is known as plastic zone for metals and fracture process zone for ceramics and some composite materials. The size of the plastic zone is denoted by r_p and represents the radius corresponding to the yield stress, cf. Fig. 6. The linear elastic stress field is valid only in K -dominant zone, for example when r_p is less than $1/25^{\text{th}}$ of the crack length a .

The crack tip displacement fields for linear elastic isotropic materials are

- for Mode I

$$\begin{aligned} u &= \frac{K_I}{2\mu} \sqrt{\frac{r}{2\pi}} \cos \frac{\theta}{2} \left(\kappa - 1 + 2 \sin^2 \frac{\theta}{2} \right) \\ v &= \frac{K_I}{2\mu} \sqrt{\frac{r}{2\pi}} \sin \frac{\theta}{2} \left(\kappa + 1 - 2 \cos^2 \frac{\theta}{2} \right) \end{aligned} \quad (12)$$

- for Mode II

$$\begin{aligned} u &= \frac{K_{II}}{2\mu} \sqrt{\frac{r}{2\pi}} \sin \frac{\theta}{2} \left(\kappa + 1 + 2 \cos^2 \frac{\theta}{2} \right) \\ v &= -\frac{K_{II}}{2\mu} \sqrt{\frac{r}{2\pi}} \cos \frac{\theta}{2} \left(\kappa - 1 - 2 \sin^2 \frac{\theta}{2} \right) \end{aligned} \quad (13)$$

- for Mode III

$$\begin{aligned} w &= \frac{K_{III}}{\mu} \sqrt{\frac{r}{2\pi}} \sin \frac{\theta}{2} \\ v &= v = 0 \end{aligned} \quad (14)$$

where μ is the shear modulus and $\kappa = 3 - 4\nu$ for plane strain and $\kappa = (3 - \nu)/(1 + \nu)$ for plane stress.

The Stress Intensity Factors are very important because under conditions of small-scale yielding, all crack front fields are dominated by the stress intensity factor. Therefore, all crack behavior like stability (will the crack tip propagate?), trajectory (in which direction will grow), and rate (how fast will grow) are controlled by the stress intensity factor and, maybe by higher order terms.

The Stress Intensity Factors could be determined analytically using complex stress functions, weight functions, Green's functions, numerically with Finite Element Method or Boundary Element Method or experimentally by strain gauges, photoelastic stress analysis, thermoelastic stress analysis.

The fracture criterion based on the SIF states that unstable fracture occurs when the stress intensity factor reaches a critical value K_{Ic} , also called fracture toughness. K_{Ic} represents the inherent ability of a material to withstand a given stress field intensity at the tip of a crack and to resist to progressive tensile crack extension. Thus a crack will propagate (under pure mode I), whenever the stress intensity factor K_I (which characterizes the strength of the singularity for a given problem) reaches a material constant K_{Ic} . Hence, under the assumptions of linear elastic fracture mechanics (LEFM), at the point of incipient crack growth

$$K_I = \beta\sigma\sqrt{\pi a} = K_{Ic} \quad (15)$$

This fracture criteria is the most commonly used in LEFM because a lot SIF's solutions are available for different cracked bodies and the fracture toughness of materials is a common mechanical property. The measured value of K_c is high for small specimen thicknesses and reaches a nearly constant lower plateau at large specimen thicknesses; this value of the critical stress intensity factor, labeled K_{Ic} , represents the plane strain fracture toughness, cf. Fig. 7.

Generally, determination of fracture toughness is carried on experimentally using standard test procedures, and will be presented in Section 2. Micromechanical models were developed based on analytical solutions (Section 3) or on finite element methods in order to predict the fracture toughness of cellular materials.

The chart of the fracture toughness versus Young modulus was plotted by Ashby, Fig. 8. The range of fracture toughness is large: from less than 0.01 to over 100 MPa m^{0.5}. At the lower end of this range are brittle materials, which, when loaded, remain elastic until they fracture. For these materials the linear-elastic fracture mechanics works well, and the fracture toughness itself is a well-defined property. At the upper end lie the hi-tough

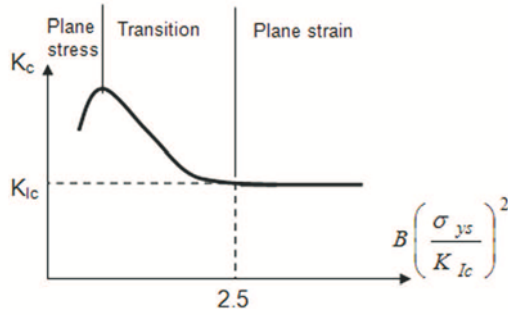


Figure 7. Variation of fracture toughness with normalized specimen thickness

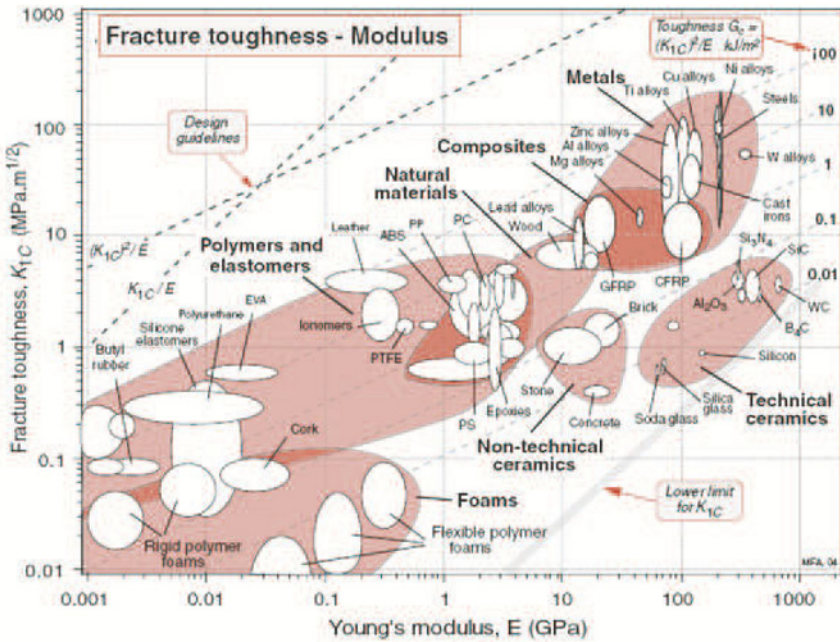


Figure 8. Fracture toughness K_{Ic} , plotted against Young's modulus, E , after Ashby (2005)

materials, all of which show substantial plasticity before they break. For these materials the Elasto-Plastic Fracture Mechanics should be applied. Cellular materials like rigid polymer foams are placed on the bottom left part in this chart, showing low fracture toughness and low Young's modulus. The lines corresponding to different values of $(K_{Ic})^2/E$ and constant K_{Ic}/E , could be used in design against fracture. The shaded band corresponding to the lower limit of K_{Ic} shows the "necessary condition" for fracture. Fracture can, in fact, occur below this limit under conditions of corrosion, or cyclic loading.

Comparing Eqs (2) and (8) it can be seen the correlation between energy release rate and stress intensity factor:

$$\mathcal{G} = \frac{K_I^2}{E} \quad \text{- for plane stress} \quad (16)$$

$$\mathcal{G} = (1 - \nu^2) \frac{K_I^2}{E} \quad \text{- for plane strain} \quad (17)$$

Design based on LEFM. Assessment of integrity and reliability of structures requires a detailed analysis of the stress and deformation that they experience. Early designs were based on strength of materials criteria which states that $\sigma = \sigma_L$ (Fig. 9), where σ_L is the limit stress, representing the ratio between yield or tensile strength and a safety factor. The Fracture

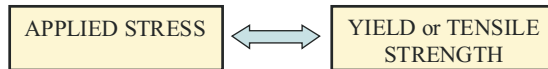


Figure 9. Classical Strength of Materials design criteria

Mechanics approach takes into account the flaw size, cf. Eq. (15).

Thus, for the design of a cracked, or potentially cracked, structure, the engineer would have to decide what design variables can be selected, as only, two of these variables can be fixed, and the third must be determined. The design variables shown in Fig. 10 are:

Material properties: fracture toughness K_{Ic} ,

Design stress level: applied stress σ ,

Flaw size: crack length a .

In assessing the safety of a cracked body, it is essential that the crack length a is properly known. In most cases it is not. Thus assumptions must be made for its value, and those assumptions are dependent upon the

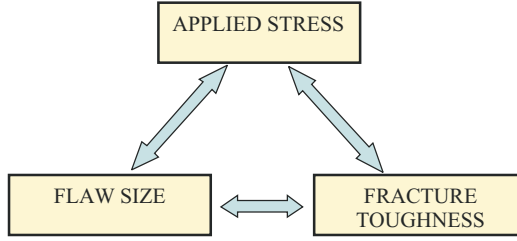


Figure 10. Fracture Mechanics design criteria

crack detection methodology adopted. The presence of a crack, equal to the smallest one that can be detected, must be assumed.

1.3 Crack tip stress and displacement fields in anisotropic materials

In many cases the behavior of the cellular materials is anisotropic. Usually, the in-plane properties differ from those in out-of-plane direction for manufactured foams. Natural cellular solids are more anisotropic (Gibson and Ashby, 1997). The generalized Hooke's Law can be expressed for an anisotropic material in the form

$$\begin{pmatrix} \varepsilon_1 \\ \varepsilon_2 \\ \varepsilon_3 \\ \varepsilon_4 \\ \varepsilon_5 \\ \varepsilon_6 \end{pmatrix} = \begin{bmatrix} a_{11} & a_{12} & a_{13} & a_{14} & a_{15} & a_{16} \\ a_{21} & a_{22} & a_{23} & a_{24} & a_{25} & a_{26} \\ a_{31} & a_{32} & a_{33} & a_{34} & a_{35} & a_{36} \\ a_{41} & a_{42} & a_{43} & a_{44} & a_{45} & a_{46} \\ a_{51} & a_{52} & a_{53} & a_{54} & a_{55} & a_{56} \\ a_{61} & a_{62} & a_{63} & a_{64} & a_{65} & a_{66} \end{bmatrix} \begin{pmatrix} \sigma_1 \\ \sigma_2 \\ \sigma_3 \\ \sigma_4 \\ \sigma_5 \\ \sigma_6 \end{pmatrix} \quad (18)$$

For this general case we have 36 independent constants a_{ij} . However, taking into account the symmetry $a_{ij} = a_{ji}$ this reduces to 21 independent constants. If the material has one plane of symmetry, it reduces to 13 independent constants. For the case of an orthogonal anisotropic material, known also orthotropic, there are three orthogonal planes of elastic symmetry and $a_{16} = a_{26} = a_{36} = a_{45} = 0$, resulting in 9 independent constants

$$\begin{pmatrix} \varepsilon_1 \\ \varepsilon_2 \\ \varepsilon_3 \\ \varepsilon_4 \\ \varepsilon_5 \\ \varepsilon_6 \end{pmatrix} = \begin{bmatrix} a_{11} & a_{12} & a_{13} & 0 & 0 & 0 \\ a_{21} & a_{22} & a_{23} & 0 & 0 & 0 \\ a_{31} & a_{32} & a_{33} & 0 & 0 & 0 \\ 0 & 0 & 0 & a_{44} & 0 & 0 \\ 0 & 0 & 0 & 0 & a_{55} & 0 \\ 0 & 0 & 0 & 0 & 0 & a_{66} \end{bmatrix} \begin{pmatrix} \sigma_1 \\ \sigma_2 \\ \sigma_3 \\ \sigma_4 \\ \sigma_5 \\ \sigma_6 \end{pmatrix} \quad (19)$$

Considering the engineering constants Young's moduluae E_1, E_2, E_3 , Poisson's ratios $\nu_{12}, \nu_{21}, \nu_{13}, \nu_{31}, \nu_{23}, \nu_{32}$ and shear moduluae G_{12}, G_{13}, G_{23} for an orthotropic material, Eq. (19) can be expressed

$$\begin{aligned}
 \varepsilon_1 &= \frac{1}{E_1}(\sigma_1 - \nu_{12}\sigma_2 - \nu_{13}\sigma_3) \\
 \varepsilon_2 &= \frac{1}{E_2}(\sigma_2 - \nu_{21}\sigma_1 - \nu_{23}\sigma_3) \\
 \varepsilon_3 &= \frac{1}{E_3}(\sigma_3 - \nu_{31}\sigma_1 - \nu_{32}\sigma_2) \\
 \gamma_{12} &= \frac{\sigma_{12}}{G_{12}} \\
 \gamma_{13} &= \frac{\sigma_{13}}{G_{13}} \\
 \gamma_{23} &= \frac{\sigma_{23}}{G_{23}}
 \end{aligned} \tag{20}$$

allowing to identify the coefficients a_{ij}

$$\begin{aligned}
 a_{11} &= \frac{1}{E_1}, a_{22} = \frac{1}{E_2}, a_{33} = \frac{1}{E_3}, \\
 a_{12} = a_{21} &= -\frac{\nu_{12}}{E_1} = -\frac{\nu_{21}}{E_2}, a_{23} = a_{32} = -\frac{\nu_{23}}{E_2} = -\frac{\nu_{32}}{E_3}, \\
 a_{13} = a_{31} &= -\frac{\nu_{31}}{E_3} = -\frac{\nu_{13}}{E_1}, \\
 a_{44} &= \frac{1}{G_{12}}, a_{55} = \frac{1}{G_{31}}, a_{66} = \frac{1}{G_{12}}
 \end{aligned} \tag{21}$$

For a transversally isotropic material, Fig. 11 like some man-made foams or corks, we have only 5 independent elastic constants

$$\left\{ \begin{array}{c} \varepsilon_1 \\ \varepsilon_2 \\ \varepsilon_3 \\ \varepsilon_4 \\ \varepsilon_5 \\ \varepsilon_6 \end{array} \right\} = \left[\begin{array}{ccccccc} a_{11} & a_{12} & a_{13} & 0 & 0 & 0 & \\ a_{21} & a_{22} & a_{23} & 0 & 0 & 0 & \\ a_{31} & a_{32} & a_{33} & 0 & 0 & 0 & \\ 0 & 0 & 0 & 2(a_{11} - a_{12}) & 0 & 0 & \\ 0 & 0 & 0 & 0 & a_{44} & 0 & \\ 0 & 0 & 0 & 0 & 0 & a_{44} & \end{array} \right] \left\{ \begin{array}{c} \sigma_1 \\ \sigma_2 \\ \sigma_3 \\ \sigma_4 \\ \sigma_5 \\ \sigma_6 \end{array} \right\}, \tag{22}$$

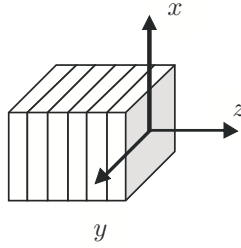


Figure 11. Transversally isotropic material

Table 2. Number of independent and nonzero coefficients

Material Type	Independent coefficients	Nonzero coefficients
General Anisotropic	21	36
Orthotropic	9	12
Transversally isotropic	5	12
Isotropic	2	12

which in terms of engineering constants become

$$\begin{aligned}
 \varepsilon_1 &= \frac{1}{E}\sigma_1 - \frac{\nu}{E}\sigma_2 - \frac{\nu'}{E'}\sigma_3 \\
 \varepsilon_2 &= \frac{1}{E}\sigma_2 - \frac{\nu}{E}\sigma_1 - \frac{\nu'}{E'}\sigma_3 \\
 \varepsilon_3 &= \frac{1}{E'}\sigma_3 - \frac{\nu'}{E'}(\sigma_1 + \sigma_2) \\
 \gamma_{12} &= \frac{2(1 + \nu)\sigma_{12}}{E} \\
 \gamma_{13} &= \frac{\sigma_{13}}{G'} \\
 \gamma_{23} &= \frac{\sigma_{23}}{G'}
 \end{aligned} \tag{23}$$

where E and ν represents the elastic properties in the plane of isotropy and E' , G' and ν' elastic properties for the plane normal to the plane of isotropy.

Table 2 presents the number of coefficients for different types of materials.

For a cracked homogeneous anisotropic material loaded in mixed mode loading (I and II) the stress field can be expressed using the stress intensity

factors in the form (Sih et al., 1965)

$$\begin{aligned}
\sigma_{xx} &= \frac{K_{Ia}}{\sqrt{2\pi r}} \Re \left[\frac{s_1 s_2}{s_1 - s_2} \left(\frac{s_2}{\sqrt{\cos \theta + s_2 \sin \theta}} - \frac{s_1}{\sqrt{\cos \theta + s_1 \sin \theta}} \right) \right] \\
&= \frac{K_{IIa}}{\sqrt{2\pi r}} \Re \left[\frac{1}{s_1 - s_2} \left(\frac{s_2^2}{\sqrt{\cos \theta + s_2 \sin \theta}} - \frac{s_1^2}{\sqrt{\cos \theta + s_1 \sin \theta}} \right) \right] \\
\sigma_{yy} &= \frac{K_{Ia}}{\sqrt{2\pi r}} \Re \left[\frac{1}{s_1 - s_2} \left(\frac{s_1}{\sqrt{\cos \theta + s_2 \sin \theta}} - \frac{s_2}{\sqrt{\cos \theta + s_1 \sin \theta}} \right) \right] \\
&= \frac{K_{IIa}}{\sqrt{2\pi r}} \Re \left[\frac{1}{s_1 - s_2} \left(\frac{1}{\sqrt{\cos \theta + s_2 \sin \theta}} - \frac{1}{\sqrt{\cos \theta + s_1 \sin \theta}} \right) \right] \\
\sigma_{xy} &= \frac{K_{Ia}}{\sqrt{2\pi r}} \Re \left[\frac{s_1 s_2}{s_1 - s_2} \left(\frac{1}{\sqrt{\cos \theta + s_2 \sin \theta}} - \frac{1}{\sqrt{\cos \theta + s_1 \sin \theta}} \right) \right] \\
&= \frac{K_{IIa}}{\sqrt{2\pi r}} \Re \left[\frac{1}{s_1 - s_2} \left(\frac{s_1}{\sqrt{\cos \theta + s_2 \sin \theta}} - \frac{s_2}{\sqrt{\cos \theta + s_1 \sin \theta}} \right) \right],
\end{aligned} \tag{24}$$

where \Re represents the real part, s_1 and s_2 are roots of the general equation (Saouma, 1997)

$$a_{11}s^4 - 2a_{16}s^3 + (2a_{12} + a_{66})s^2 - 2a_{26}s + a_{22} = 0 \tag{25}$$

in the form $s_j = \alpha_j + i\beta_j$, for $j = 1, 2$, a_{ij} are the components of the compliant matrix.

The most important observation is that for the anisotropic case like in the isotropic case the stress field has a singularity of order $r^{-0.5}$. Regarding the stress intensity factors values for anisotropic materials differ from those for isotropic materials (Murakami, 1987).

The displacement field for mode I loading conditions can be expressed in the form

$$\begin{aligned}
u_1 &= K_{Ia} \sqrt{\frac{2r}{\pi}} \Re \left\{ \frac{1}{s_1 - s_2} \left[s_1 p_2 \sqrt{\cos \theta + s_2 \sin \theta} - s_2 p_1 \sqrt{\cos \theta + s_1 \sin \theta} \right] \right\}, \\
v_1 &= K_{Ia} \sqrt{\frac{2r}{\pi}} \Re \left\{ \frac{1}{s_1 - s_2} \left[s_1 q_2 \sqrt{\cos \theta + s_2 \sin \theta} - s_2 q_1 \sqrt{\cos \theta + s_1 \sin \theta} \right] \right\}, \\
w_1 &= 0
\end{aligned} \tag{26}$$

with

$$p_j = a_{11}s_j^2 + a_{12} - a_{16}s_j, \quad q_j = a_{12}s_j + \frac{a_{22}}{s_j} - a_{26}, \quad j = 1, 2 \tag{27}$$

For orthotropic materials the characteristic equation becomes

$$s^4 + \left(\frac{E_1}{G_{12}} - 2\nu_{12} \right) s^2 + \frac{E_1}{E_2} = 0 \tag{28}$$

A study of the solutions for the characteristic equation is presented by Saouma (1997).

2 Experimental Determination of Fracture Toughness of Foam Materials

It is well known that the foam crushes in compression, Fig. 12 (*left*), while in tension fails by propagating of single crack, Fig. 12 (*right*). Most of the

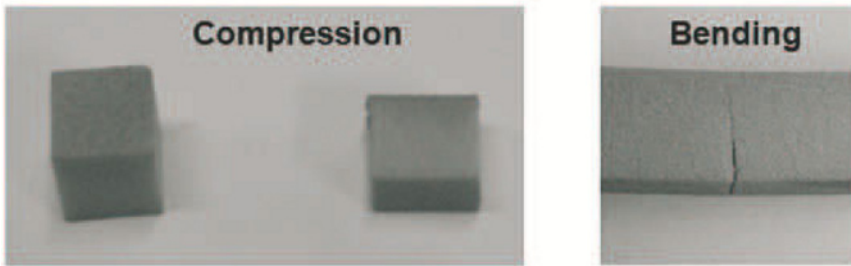


Figure 12. Mechanisms of foam damage in compression and bending

rigid polymer foams have a linear - elastic behavior in tension up to fracture, and a brittle fracture, so they can be treated using fracture criteria's of Linear Elastic Fracture Mechanics (LEFM). The case of metallic foams with elasto-plastic fracture behavior will not be treated here, but was extensively investigated during the last 10 years by McCullough et al. (1999); Ashby et al. (2000); Olurin et al. (2000); Andrews and Gibson (2001); Fleck et al. (2001); Motz and Pippan (2001); Motz (2002); Degischer and Kriszt (2002); Onck et al. (2005).

Methods for testing of polymeric foams are reviewed by Landrock (1995); Brown (1999, 2002); Ward and Sweeney (2004). Different procedures for determination of fracture toughness for cellular materials were developed for flexible and rigid foams.

2.1 Tear Test for Flexible Cellular Materials

This test method is standardized by ASTM D 3574-03: Standard Test Methods for Flexible Cellular Materials-Slab, Bonded, and Molded Urethane Foams (Test F), ASTM D 3575-00: Standard Test Methods for Flexible Cellular Materials Made from Olefin Polymers (Test G), and BS EN ISO 8067-89: Flexible Cellular Polymeric Materials - Determination of Tear Strength.

Scope. The test method covers determination of the tear propagation resistance of foam, by measuring the tear resistance under the conditions of this particular test. The tear strength represents the force needed to rip a foam specimen.

Apparatus. The tear resistance should be measured on a power-driven apparatus which will indicate the force at which fracture of the specimen takes place. An automatic machine can be used which draws the actual curve, or, a style or scale can be used having an indicator that remains at the point of maximum force after fracture.

Test Specimens. The test specimens shall be a block shape free of skin, voids, and densification lines, as shown in Fig. 13. They may be cut on

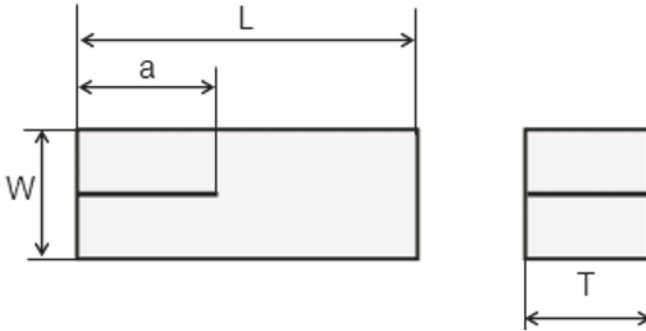


Figure 13. Tear strength specimens

a saw or die cut from sheet material so that the sides are parallel and perpendicular to each other. The block dimensions should be $T = W = 25$ mm, $L = 125$ mm (after EN ISO 8067-89). A nominal $a = 50$ mm cut shall be produced, with a razor blade or knife, in one side as shown in Fig. 13. The tests should be performed at least 72 hours after manufacture at room temperature. At least, three specimens per sample must be tested. The values reported are to be the mean of those tested.

Procedure. The specimen legs are clamped and pulled apart with a speed of 50 to 500 mm/min. After the fracture of the specimen, or after at least a 50-mm length is torn, record the maximum force in Newtons and note also the thickness of the specimen

Calculation. Calculate the tear strength from the maximum force registered on the testing machine and the average thickness of the specimen T , as follows

$$R = \frac{F_{\max}}{T} 10^3, \quad (29)$$

where R is the tear strength in [N/m], F_{\max} - maximum force, [N], T - thickness, [mm]. Some Tear Strength results together with other mechanical characteristics of flexible ethylene-vinyl acetate (EVA) foam are presented in Table 3 from www.rueylung.com.tw/products/EVA_Foam.

2.2 Standard Test Methods for Plane-Strain Fracture Toughness and Strain Energy Release Rate of Plastic Materials

The test procedure for determining the plane strain fracture toughness of plastic materials is standardized by the American Society for Testing and Materials, ASTM D5045-99 which is based on ASTM E399-97 Test Method for Plane-Strain Fracture Toughness of Metallic Materials, but includes specific consideration for plastic materials.

Scope. The test method is designed to determine the toughness of plastics in terms of the critical stress intensity factor, K_{Ic} , and the energy per unit area of crack surface or critical strain energy release rate, \mathcal{G}_{Ic} , at fracture initiation. Two types of specimens are proposed: Single Edge Notch Bending (SENB) specimen and Compact Tension (CT) specimen. Linear elastic behavior under plane strain conditions is assumed, certain restrictions on linearity and specimen dimensions are considered in order to validate the experimental results

Apparatus. A constant displacement rate device shall be used such as an electromechanical, screw-driven machine, or a closed loop, feedback-controlled servo-hydraulic load frame. For SENB, a rig with either stationary or moving rollers of sufficiently large diameter to avoid excessive plastic indentation is required. A suitable arrangement for loading the SENB specimen is presented in Fig. 14 (*left*). A loading clevis suitable for loading compact tension specimens is shown in Fig. 14 (*right*). Loading is produced through pins on the specimen holes (Fig. 14 (*right*)). An accurate displacement measurement must be obtained to assure accuracy of the \mathcal{G}_{Ic} value.

For either SENB or CT specimen configurations, the displacement measurement can be performed using the machine's position transducer. The load-displacement data must be corrected for system compliance, loading-

Table 3. Mechanical characteristics of EVA foam materials

Foam Type	L-2500	C-1600	C-3000	H-25	H-35	A-25
Density [kg/m ³]	21-27	35-41	23-29	65-75	70-80	80-90
Original Sheet Thickness [mm]	80	80	80	36	32	38
Tensile Strength [MPa]	0.196	0.314	0.274	0.932	1.157	0.932
Elongation at Break [%]	180	180	340	220	160	120
Tear Strength [N/m]	1863	2353	2059	3334	3726	3236
Compressive Strength at 25% Deflection [MPa]	0.039	0.059	0.029	0.069	0.078	0.069
Compressive Strength at 50% Deflection [MPa]	0.098	0.127	0.078	0.147	0.176	0.157

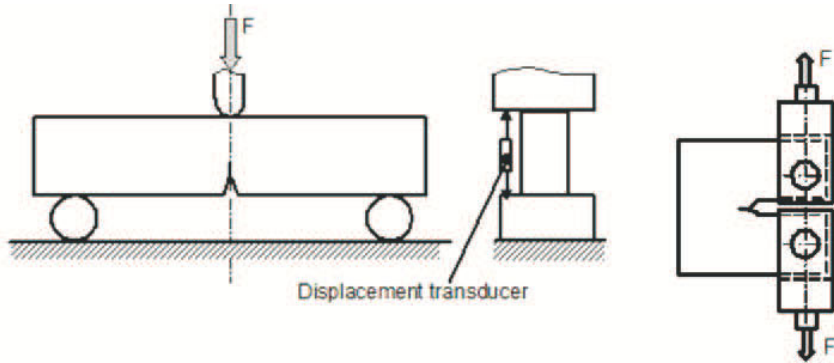


Figure 14. Arrangement of loadings: SENB specimen (left), CT specimen (right)

pin penetration and sample compression by performing a calibration of the testing system.

If an internal displacement transducer is not available, or has insufficient precision, then an externally applied displacement-measuring device may be used as illustrated in Fig. 14 (*right*) for the SENB configuration. For CT specimens, a clip gage can be mounted across the loading pins. For both the SENB and CT specimens, the displacement should be taken at the load point.

Test Specimens. SENB and CT geometries are recommended over other configurations because these have predominantly bending stress states which allow smaller specimen sizes to achieve plane strain conditions. If the material is supplied in the form of a sheet, the specimen thickness, B , should be identical with the sheet thickness. The criteria require that B must be sufficient to ensure plane strain and that $(W - a)$ be sufficient to avoid excessive plasticity in the ligament. If $(W - a)$ is too small and non-linearity in loading occurs, then increasing the W/B ratio to a maximum of 4 can be attempted for SENB specimens. Initially, prepare a sharp notch by machining. Subsequently, initiate a natural crack by inserting a fresh razor blade and tapping. If a natural crack cannot be successfully initiated by tapping, a sufficiently sharp crack can alternatively be generated by sliding or sawing a new razor blade across the notch root. The dimensions of standard specimens are shown in Fig. 15. At least three specimens for each material condition should be tested.

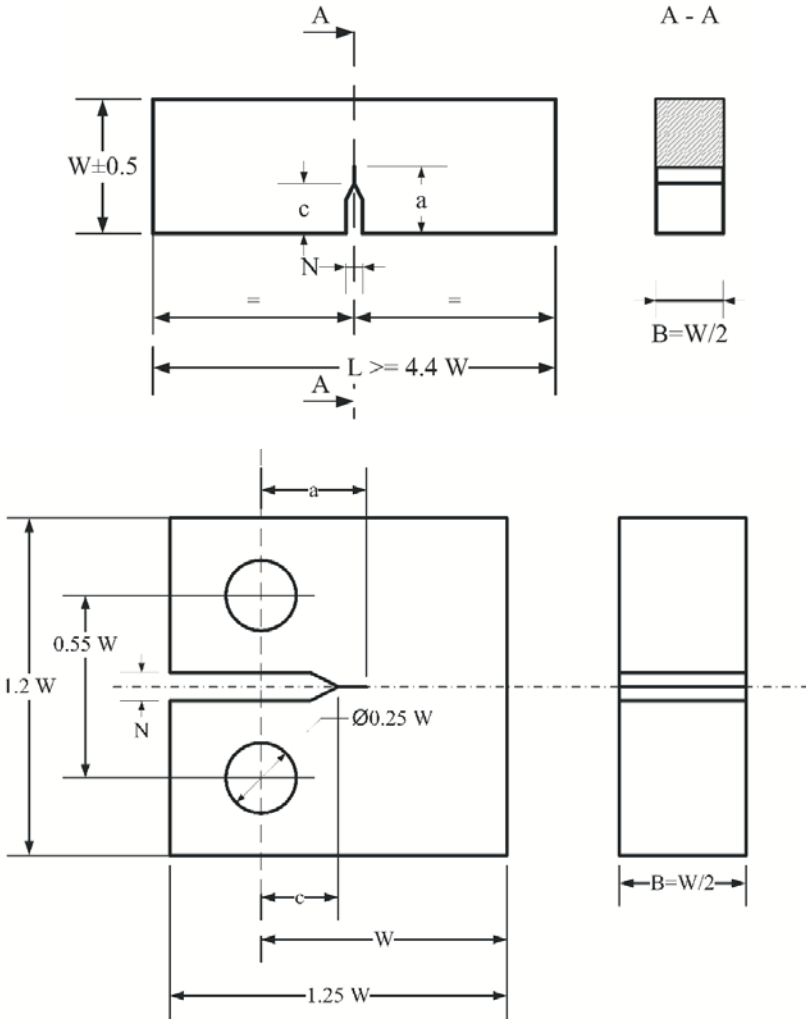


Figure 15. Specimens configuration for D 5045-99 test: SENB specimen (up), CT specimen (down)

Procedure. Since plastics are viscoelastic materials, it is necessary to specify both the temperature and time scale under which the result was obtained. It is recommended that tests be performed at a temperature of 23°C, and a crosshead rate of 10 mm/min.

The load versus loading-point displacement curve is recorded during test. In the ideal case this is a linear diagram with an abrupt drop of load to zero at the instant of crack growth initiation. In some cases this occurs and K_Q can be found from the maximum load.

The determination of G_{Ic} requires an accurate integration of the load versus loading point displacement curve, which necessitates an accurate displacement determination using a displacement transducer.

Calculation and results interpretation. Calculation value of stress intensity factors K_Q is obtained based on force-displacement curve, cf. Fig. 16. First, draw a straight line (AB) to determine the initial compliance

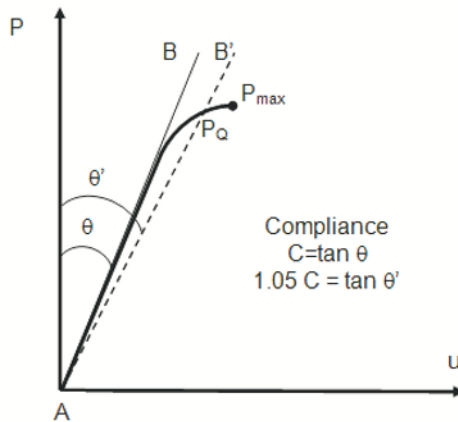


Figure 16. Typical load - displacement curve

$C = \tan \theta$, which represents the slope of line (AB). Draw a second line (AB') with the compliance 5% greater than that of line (AB). If the maximum load that the specimen was able to sustain, P_{max} , falls within lines (AB) and (AB'), use P_{max} to calculate K_Q . If P_{max} falls outside line (AB) and line (AB'), then use the intersection of line (AB') and the load curve as P_Q . Furthermore, if $P_{max}/P_Q < 1.1$ use P_Q in the calculation of K_Q . However, if $P_{max}/P_Q > 1.1$ the test is invalid.